THE JOURNAL OF PHYSICAL CHEMISTRY A
A JOURNAL OF THE AMERICAN CHEMICAL SOCIETY

pubs.acs.org/JPCA Article

Using Diffusion Monte Carlo Wave Functions to Analyze the Vibrational Spectra of $H_7O_3^+$ and $H_9O_4^+$

Published as part of The Journal of Physical Chemistry virtual special issue "125 Years of The Journal of Physical Chemistry".

Ryan J. DiRisio, Jacob M. Finney, Laura C. Dzugan, Lindsey R. Madison, and Anne B. McCoy*

Cite This: *J. Phys. Chem. A* 2021, 125, 7185–7197 Read Online

ACCESS | Metrics & More | Article Recommendations | Supporting Information

ABSTRACT: An approach for evaluating spectra from ground state probability amplitudes (GSPA) obtained from diffusion Monte Carlo (DMC) simulations is extended to improve the description of excited state energies and allow for coupling among vibrational excited states. This approach is applied to studies of the protonated water trimer and tetramer, and their deuterated analogs. These ions provide models for solvated hydronium, and analysis of these spectra provides insights into spectral signatures of proton transfer in aqueous environments. In this approach, we obtain a separable set of internal coordinates from the DMC ground state probability amplitude. A basis is then developed from products of the DMC ground state wave function and low-order polynomials in these internal coordinates. This approach provides a compact basis in which the Hamiltonian and dipole moment matrix are evaluated and used to obtain the spectrum. The resulting spectra are in good agreement with experiment and in many cases provide comparable agreement to the results obtained using much larger basis sets. In addition, the compact basis allows for interpretation of the spectral features and how they evolve with cluster size and deuteration.

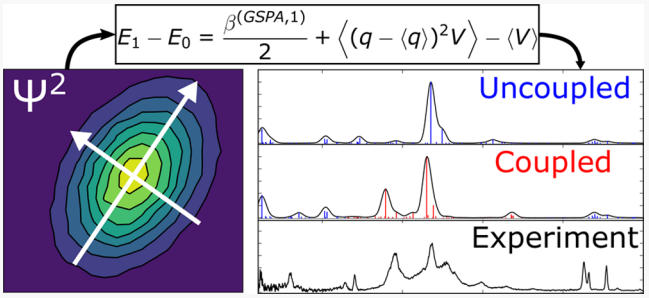

INTRODUCTION

The study of the proton transfer mechanism in water is an important area of investigation. Advances in experimental techniques have allowed for the study of this mechanism in bulk systems,[1,2] the air/water interface,[3−5] nanodroplets and reverse micelles,[6,7] and gas-phase water clusters.[8−15] Cold, protonated water clusters provide model systems through which one can experimentally and theoretically interrogate the underlying physics of an excess proton in a known environment. In particular, vibrational spectroscopy of these systems allows for the direct interrogation of the motions that underpin proton transfer.

Experimental and theoretical studies of $H^+(H_2O)_{n=1-4}$ have demonstrated that the incorporation of nuclear quantum effects is essential to obtain an accurate description of the vibrational dynamics and spectroscopy of these systems.[13,15−24] Additionally, these studies show how the position, width and structure of the spectral feature that corresponds to the transition to the state with one quantum of excitation in a hydrogen-bonded OH stretch in the hydronium core is modulated by the cluster size and solvation environment.[10] Much can be learned from the analysis and theoretical reproduction of the spectra of the protonated water clusters. As chemists, an important aspect of this type of work is in the ability to make connections between the features in the spectrum and the underlying bond strengths and structure of the ion that is being studied.

Analysis of changes to the vibrational frequency of the shared proton stretch with cluster size and structure has shown that the changes reflect the couplings between the OH stretch vibrations that lead to proton transfer and various intra- and intermolecular vibrations of the donating hydronium ion and the accepting water molecule. These couplings are also responsible for the evolution of the spectral envelope of the feature associated with the shared proton stretch. These large couplings make protonated water clusters challenging systems for computational approaches, such as vibrational perturbation theory (VPT2) or reduced dimensional treatments, which rely on a good zero-order description.[19,20,24,25] An alternative approach involves the use of large basis set calculations, e.g. vibrational self-consistent field/vibrational configuration inter-

Received: June 7, 2021
Revised: July 23, 2021
Published: August 16, 2021

https://doi.org/10.1021/acs.jpca.1c05025
J. Phys. Chem. A 2021, 125, 7185–7197

action (VSCF/VCI) approaches. Yu and Bowman have performed VSCF/VCI calculations of the spectra of the protonated water trimer ($H_7O_3^+$) and tetramer ($H_9O_4^+$) using a Hamiltonian that is expressed in the normal mode coordinates of the ion of interest, focusing on the 18 and 24 vibrations that are expected to be responsible for the spectral features in $H_7O_3^+$ and $H_9O_4^+$,[13,20,22] respectively. The large couplings among the normal modes meant that large basis sets were needed to obtain converged results. The large basis along with a coordinate choice that did not follow the curvilinear nature of the molecular vibrations made the interpretation of the resulting spectra challenging.[13,15,20,22,23,26] This problem is most severe in the low energy region of the spectrum, which is dominated by large amplitude, low-frequency motions. The exclusion of the low-frequency vibrations in the VSCF/VCI analysis renders this spectral region inaccessible by this approach, while the large cubic and quartic terms in the expansion of the Hamiltonian lead to divergent behavior in VPT2 calculations. For this region, quasiclassical calculations as well as classical and ring polymer molecular dynamics calculations have been used to study this region of the spectrum.[15,23]

The focus of the present study will be on the examination of the molecular vibrations in $H_7O_3^+$ and $H_9O_4^+$, and their deuterated analogs. The vibrational spectra of $H_7O_3^+$ and $H_9O_4^+$ are quite similar, both in the low frequency region (200−1000 cm^{-1}) and much of the region that corresponds to the $\Delta n = 1$ transitions of the OH stretches and bends (1000−4000 cm^{-1}). The main spectroscopic differences between the two systems are in the shared proton stretching region, where the spectrum of $H_7O_3^+$ has a series of peaks from approximately 1800−2500 cm^{-1}, and the shared proton stretching region of $H_9O_4^+$ consists of a single, broad peak centered at 2650 cm^{-1}.

Previous theoretical studies of $H_7O_3^+$ have shown that the series of intense peaks in the region of the $\Delta n = 1$ transition of the shared proton stretch result from intensity borrowing.[13,19,22,24,26] Specifically, there are a number of vibrational states that are nearly degenerate with the state with one quantum of excitation in the shared proton stretching mode, which can mix with that state. The importance of intensity borrowing among several states makes the interpretation of this region of the spectrum difficult. It also results in a large difference in the shape of the spectral envelope of this region upon deuteration. Despite the large amplitude nature of the vibrations, degenerate forms of VPT2, which are based on normal mode Hamiltonians expressed in internal[25] and Cartesian[24] coordinates as well as VSCF/VCI calculations[13] all provide reasonable reproductions of the spectral envelopes for $H_7O_3^+$ and $D_7O_3^+$. An analysis of the states that contribute to the peaks in the calculated spectra in the region of the $n = 1$ level in the shared proton stretch shows that many of these transitions involve two quanta of excitation in low frequency modes.

While there are fewer peaks in the shared proton region of the spectrum in $H_9O_4^+$ and $D_9O_4^+$, Bowman and Yu assigned the broad shared proton stretch feature as a series of complicated combination bands involving the shared proton stretching vibration and rotations and bends of the hydronium core, and the results of degenerate VPT2 calculations indicated that the band was composed of the shared proton stretching mode as well as umbrella and hydronium bend combinations.[20,27]

While progress has been made in interpreting the spectra of these systems, the analysis is sensitive to the choice of coordinates. The observation that degenerate VPT2 calculations based on states with up to two quanta of excitation provide a reasonable description of the spectra of $H_7O_3^+$ and $H_9O_4^+$[14,24,25] leads us to conclude that if we can identify a good set of coordinates, we may be able to obtain a reasonable description of the spectrum using a much smaller basis than is required for the previous VSCF/VCI calculations.

To explore this possibility, we will use insights gained from the ground state probability amplitudes for $H_7O_3^+$ and $H_9O_4^+$, which were obtained from diffusion Monte Carlo (DMC) simulations.[28] DMC is a stochastic method in which an ensemble of localized functions, referred to as walkers, randomly samples the potential energy surface for the system of interest. The DMC ground state wave function is represented by the density of walkers near the configuration of interest. While DMC provides a powerful approach for obtaining information about the vibrational ground state wave function and energy of a molecular cluster, extracting information about excited states presents significant challenges. First, without further modification to the algorithm,[29] each excited state must be calculated independently, and each state is described by distinct ensembles of walkers. Further, the evaluation of these excited states requires knowledge of the associated nodal surface, which can become quite complicated when large amplitude vibrations are involved.[13,30,31] The fact that distinct sets of walkers are used to describe each state also makes the evaluation of matrix elements of the Hamiltonian or dipole moment difficult.[32]

To circumvent these challenges, in the present study, we explore an approach in which we use the DMC ground state probability amplitude (GSPA) to generate a set of coordinates, which we then use to calculate the vibrational spectra of $H_7O_3^+$, $H_9O_4^+$, and their deuterated analogs in a small basis set calculation. The GSPA approach was outlined in a pair of studies on $H_3O_2^-$ and $H_5O_2^+$,[33,34] and has also been applied to calculations of the H_2 stretch frequencies in H_5^+.[35] In this approach, excited states are approximated as products of polynomials that are functions of displacements of internal coordinates, which are obtained from the ground state probability amplitude, and the DMC ground state wave function. This approach has an advantage over large basis set techniques in that the interpretation of the results is simplified by the use of a smaller, carefully constructed basis, which were shown to provide surprisingly accurate results in the earlier studies. In this work, we introduce several extensions to the previously described approaches. The first focuses on improving the description of states with two quanta of vibrational excitation. We test this extension for a series of Morse oscillators as well as a calculation of the excited state energies of H_3O^+. We also consider general strategies for selecting the internal coordinates on which the approximation is based. Finally, we extend the approach to account for strong coupling of the shared proton stretch to nearby nearly degenerate states.

METHODS

Overview of DMC. In the present study, we use the GSPA approach to evaluate the spectra of $H_7O_3^+$, $D_7O_3^+$, $H_9O_4^+$, and $D_9O_4^+$, as well as the excited state energies of H_3O^+. As inputs for these calculations, we use the ground state probability amplitudes that were obtained as part of a previously reported

https://doi.org/10.1021/acs.jpca.1c05025
J. Phys. Chem. A 2021, 125, 7185−7197

DMC study of these ions,[28] where we used guided DMC simulations to obtain snapshots of $f = \Phi_0\Psi_T$. In guided DMC studies, f is represented by an ensemble of localized functions, referred to as walkers, Φ_0 is the ground state wave function of the ion of interest, and Ψ_T is a guiding function. Each walker is described by $3N$ Cartesian coordinates, $\mathbf{x}$, which represents a geometry of the N-atomic molecule of interest, and has an associated weight, w. The ensemble of walkers is propagated in imaginary time, $\tau = it/\hbar$, over a series of short time intervals, $\Delta\tau$, until the simulation has equilibrated. At that time, the density of walkers near $\mathbf{x}$ provides the value of $f(\mathbf{x})$. Once the simulation has equilibrated, we collected snapshots of f periodically during the remainder of the simulation.

The probability density associated with Φ_0 was obtained from these snapshots using descendant weighting.[31] In this approach, the value of Φ_0/Ψ_T at the coordinates of the jth walker is equated to the weight of the walker in the ensemble at some later time, τ'. Operationally, the descendant weight is calculated using

$$d_j(\tau) = \frac{w_j(\tau')}{w_j(\tau)} \tag{1}$$

Based on this expression for d_j, the expectation value of an arbitrary multiplicative operator, A can be evaluated using Monte Carlo integration,

$$\langle A\rangle = \frac{\sum_{j=1}^{N_w} A(\mathbf{x}_j(\tau))w_j(\tau)d_j(\tau)}{\sum_{j=1}^{N_w} w_j(\tau)d_j(\tau)} = \frac{\sum_{j=1}^{N_w} A(\mathbf{x}_j(\tau))w_j(\tau')}{\sum_{j=1}^{N_w} w_j(\tau')} \tag{2}$$

where N_w is the number of walkers in the ensemble. Additional details of the implementation of the DMC calculations are provided in ref 28 and the Supporting Information.

Implementation of the GSPA Approach. In a pair of earlier studies, we described an approach for approximating the excited state energies and wave functions based on the ground state probability amplitude obtained using DMC.[33,34] For the present applications, we developed a slightly modified version of this approach. As in earlier studies, we will use approximate expressions for the excited state wave functions. Since we will be focusing on states with up to two quanta of excitation, these states are denoted as $|\Phi_{n_i=l,n_j=m}\rangle$, where i and j represent the modes that are being excited, and l and m provide the number of quanta of excitation in modes i and j, respectively.

Within this approximation, $|\Phi_{n_i=l,n_j=m}\rangle$ is expressed as

$$|\Phi_{n_i=l,n_j=m}\rangle \approx \mathrm{P}_{i,j}^{(l,m)}(q_i, q_j)|\Phi_0\rangle \tag{3}$$

where

$$\mathrm{P}_{i,j}^{(l,m)}(q_i, q_j) = \sum_{k=0}^{l}\sum_{k'=0}^{m} c_{i,j}^{(k,k')}(q_i - \langle q_i\rangle)^k(q_j - \langle q_j\rangle)^{k'} \tag{4}$$

For states that involve excitation in one mode, the coefficients are determined by the requirement that

$$\langle\Phi_{n_i=l,n_j=0}|\Phi_{n_i=l',n_j=0}\rangle = 0 \tag{5}$$

for all $l' < l$. Based on these requirements,

$$\mathrm{P}_{i,j}^{(1,0)}(q_i, q_j) \equiv \mathrm{P}_i^{(1)}(q_i) = q_i - \langle q_i\rangle \tag{6}$$

and

$$\mathrm{P}_{i,j}^{(2,0)}(q_i, q_j) \equiv \mathrm{P}_i^{(2)}(q_i) = \frac{-(q_i - \langle q_i\rangle)^2}{\langle(q_i - \langle q_i\rangle)^2\rangle} + \frac{\langle(q_i - \langle q_i\rangle)^3\rangle(q_i - \langle q_i\rangle)}{\langle(q_i - \langle q_i\rangle)^2\rangle^2} + 1 \tag{7}$$

For states in which $n_i = 1$ and $n_j = 1$,

$$\mathrm{P}_{i,j}^{(1,1)}(q_i, q_j) = (q_i - \langle q_i\rangle)(q_j - \langle q_j\rangle) \tag{8}$$

The vibrational modes $\{\mathbf{q}\}$ are formed from linear combinations of $3N - 6$ carefully chosen internal coordinates, $\mathbf{r} - \langle\mathbf{r}\rangle$. The transformation matrix that rotates the internal coordinates to q-coordinates is the eigenvectors of the mass-weighted matrix of second moments $\mathbf{M}^{\mathrm{MW}}$, where

$$\mathbf{M}^{\mathrm{MW}} = \mathbf{G}^{-1/2}\mathbf{M}\mathbf{G}^{-1/2} \tag{9}$$

$$\mathrm{M}_{ij} = \langle(r_i - \langle r_i\rangle)(r_j - \langle r_j\rangle)\rangle \tag{10}$$

and $\mathbf{G}$ in eq 9 represents the Wilson $\mathbf{G}$-matrix[36] the elements of which are evaluated numerically using

$$\mathrm{G}_{ij} = \left\langle \sum_{k=1}^{3N} \frac{\partial r_i}{\partial x_k}\frac{1}{m_k}\frac{\partial r_j}{\partial x_k} \right\rangle \tag{11}$$

Finally, m_k is the atomic mass associated with x_k, and all expectation values are taken over $|\Phi_0\rangle$. It should be noted that based on the above definitions $\langle\mathbf{q}\rangle = 0$, and this definition of the q-coordinates will recover the usual normal mode coordinates in the limit of a harmonic Hamiltonian. The above definitions ensure that the ground state and all of the states with one quantum of excitation are mutually orthogonal as are states with different amounts of excitation in a given mode. Additionally, all excited states are orthogonal to the ground state. On the other hand, excited states are generally not orthogonal to each other. This will become important if we wish to introduce couplings between the approximate excited states.

To calculate the transition energy from the ground state, we need to evaluate

$$E_{n_i,n_j} - E_0 = (\langle T\rangle_{i,j}^{(l,m)} - \langle T\rangle_{i,j}^{(0,0)}) + (\langle V\rangle_{i,j}^{(l,m)} - \langle V\rangle_{i,j}^{(0,0)}) \tag{12}$$

where for an operator, $A = T$ or V,

$$\langle A\rangle_{i,j}^{(l,m)} = \langle\Phi_{n_i=l,n_j=m}|A|\Phi_{n_i=l,n_j=m}\rangle \tag{13}$$

Since the potential is a multiplicative operator,

$$\langle V\rangle_{i,j}^{(l,m)} = \frac{\langle(\mathrm{P}_{i,j}^{(l,m)})^2 V\rangle}{\langle(\mathrm{P}_{i,j}^{(l,m)})^2\rangle} \tag{14}$$

and the potential energy of each walker is evaluated using the many-body surface reported by Bowman and co-workers.[26]

The evaluation of $\langle T\rangle_{i,j}^{(l,m)} - \langle T\rangle_{i,j}^{(0,0)}$ is more complicated since an ensemble of localized functions in $3N$ dimensions is used to represent $\Phi_0\Psi_T$. While division by Ψ_T is straightforward, differentiation of Φ_0 is not. Rather than trying to differentiate Φ_0 numerically, we turn to insights from the harmonic oscillator expressed in terms of mass weighted coordinates, Q, and their conjugate momentum, P, where

$$\langle n|P^2|n\rangle - \langle 0|P^2|0\rangle = \beta n \tag{15}$$

https://doi.org/10.1021/acs.jpca.1c05025
J. Phys. Chem. A 2021, 125, 7185−7197

and

$$\langle n|Q^2|n\rangle - \langle 0|Q^2|0\rangle = \frac{n}{\beta} \tag{16}$$

Additionally, for the harmonic oscillator,

$$\langle n|T|n\rangle - \langle 0|T|0\rangle = \frac{\beta n}{2} \tag{17}$$

Here, the harmonic Hamiltonian is expressed in mass-weighted coordinates and $\hbar = 1$, $\beta = \omega$.

In the GSPA approach, we use eq 17 to evaluate the kinetic contribution to the energy, but instead of equating β to the harmonic frequency, we treat $\beta_i^{(\mathrm{GSPA},n)}$ as a parameter, which depends on the number of quanta of excitation in mode i. The expressions for $\beta_i^{(\mathrm{GSPA},n)}$ are evaluated by using relationships between $\langle Q^l\rangle$ and β, which are also based on a harmonic system. Specifically, for transitions to states with one and two quanta of excitation in the ith mode, we use

$$\beta_i^{(\mathrm{GSPA},1)} = \frac{\langle q_i^2\rangle}{\langle q_i^4\rangle - \langle q_i^2\rangle^2} \tag{18}$$

and

$$\beta_i^{(\mathrm{GSPA},2)} = \sqrt{\frac{8\langle q_i^4\rangle}{\langle q_i^8\rangle - \langle q_i^4\rangle^2}} \tag{19}$$

respectively. The above definition of $\beta^{(\mathrm{GSPA},1)}$ has been shown to provide accurate energies for transitions with $\Delta n = 1$ in $H_3O_2^-$ and $H_5O_2^+$, but it is less accurate for higher levels of vibrational excitation.[33,34] The loss of accuracy with vibrational excitation, and the need for expressions $\beta^{(\mathrm{GSPA})}$ that depend on the number of quanta of excitation, can be traced to the fact that in anharmonic systems most of the anharmonicity is in $\langle T\rangle_n$, while $\langle V\rangle_n$ is much less sensitive to the anharmonicity. For a Morse oscillator, where

$$E_n - E_0 = n\omega - n(n+1)\omega x \tag{20}$$

one can show that $\langle V\rangle_n - \langle V\rangle_0 = n\omega/2$, which is the same as the harmonic value, while $\langle T\rangle_n - \langle T\rangle_0 = n\omega/2 - n(n+1)\omega x$.[37] Letting the expression for $\beta_i^{(\mathrm{GSPA},n)}$ depend on the value of n allows us to account for the higher order terms in $\langle T\rangle$.

To evaluate intensities within the GSPA approach, we also need the matrix elements of the dipole operator, from which we calculate the transition dipole moment. These calculations for $H_7O_3^+$ and $H_9O_4^+$ are performed using the many-body dipole surface reported by Bowman and co-workers.[26] Following the above discussion,

$$\langle \Phi_{n_i=l,n_j=m}|\vec{\mu}|\Phi_{n_i=0,n_j=0}\rangle \approx \frac{\langle (\mathrm{P}_{i,j}^{(l,m)}\vec{\mu}\rangle}{\sqrt{\langle (\mathrm{P}_{i,j}^{(l,m)})^2\rangle}} \tag{21}$$

Introducing Couplings in the GSPA Approach. While the energies obtained by the approach described above provide good approximations to the excited state energies, the excited states themselves are not eigenstates of the vibrational Hamiltonian. To account for the coupling of these zero-order states, we construct a reduced-dimensional Hamiltonian **H** and the corresponding overlap matrix **S**. The diagonal elements of the Hamiltonian matrix are the energies, described above, and the diagonal elements of the overlap matrix are 1. The off-diagonal elements are given by

$$\mathbf{S}_{n,n'} = \langle \Phi_{n_i=l,n_j=m}|\Phi_{n_{i'}=l',n_{j'}=m'}\rangle = \frac{\langle \mathrm{P}_{i,j}^{(l,m)}\mathrm{P}_{i',j'}^{(l',m')}\rangle}{\sqrt{\langle (\mathrm{P}_{i,j}^{(l,m)})^2\rangle\langle (\mathrm{P}_{i',j'}^{(l',m')})^2\rangle}} \tag{22}$$

$$\mathrm{H}_{n,n'} = \langle \Phi_{n_i=l,n_j=m}|V - \langle V\rangle|\Phi_{n_{i'}=l',n_{j'}=m'}\rangle = \frac{\langle \mathrm{P}_{i,j}^{(l,m)}V\mathrm{P}_{i',j'}^{(l',m')}\rangle - \langle V\rangle\langle \mathrm{P}_{i,j}^{(l,m)}\mathrm{P}_{i',j'}^{(l',m')}\rangle}{\sqrt{\langle (\mathrm{P}_{i,j}^{(l,m)})^2\rangle\langle (\mathrm{P}_{i',j'}^{(l',m')})^2\rangle}} \tag{23}$$

The above expression for $H_{n,n'}$ includes only contributions from the potential energy. While there should also be kinetic contributions to these terms, we have found that they are small compared to the contributions from the potential energy.

The energies and wave functions, $|\Phi^{\mathrm{coup}}\rangle$, in the coupled representation can then be obtained by solving the generalized eigenvalue problem

$$\mathbf{H}|\Phi^{\mathrm{coup}}\rangle = E\mathbf{S}|\Phi^{\mathrm{coup}}\rangle \tag{24}$$

Using these eigenvectors, we can obtain the intensities of the transitions from the ground state to these mixed states.

RESULTS AND DISCUSSION

The discussion that follows will be divided into several parts. We will start by assessing the numerical accuracy of the expressions for $\beta^{(\mathrm{GSPA},n)}$, which are provided in eqs 18 and 19, by evaluating the excited state energies for a series of Morse oscillators with varying amounts of anharmonicity. We next consider the coordinates that are to be used to describe the protonated water systems and apply the GSPA technique to the calculation of spectra of these ions. We first use the GSPA approach to evaluate the energies of excited states of H_3O^+ with one and two quanta of excitation. These energies are compared to the results of VSCF/VCI calculations based on the same potential surface.[38,39] Using the insights gained from these calculations on H_3O^+, we turn to the calculated spectra of $H_7O_3^+$ and $H_9O_4^+$ and their deuterated analogs. All reported spectra that are calculated using the GSPA approach have been convoluted with Gaussian functions. The calculated transition energies and intensities between 1000 to 4000 cm^{-1} have been convoluted with Gaussians with $\sigma = 25$ cm^{-1}, while between 200 and 1500 cm^{-1} the calculated transitions have been convoluted with Gaussians with $\sigma = 10$ cm^{-1}. The relative intensity is obtained by normalizing the most intense feature in the displayed spectral region to 1.

Evaluation of the Kinetic Energy. The kinetic energy expression used in the GSPA technique is derived from the expressions of expectation values of kinetic energy for the nth state of the one-dimensional Harmonic oscillator, where $\langle T\rangle_n - \langle T\rangle_0 = n\beta/2$. In eqs 18 and 19, we introduced expressions for evaluating $\beta^{(\mathrm{GSPA},n)}$ for $n = 1$ and 2, which can be used to obtain an approximation to the kinetic contribution to the transition energy. To explore the accuracy of this approximation, we use a series of one-dimensional Morse oscillators, for which

$$E_n = \omega(n + 1/2) - \omega x(n + 1/2)^2 \tag{25}$$

and the transition energies are described in eq 20. For this series of Morse oscillators, $\omega = 3000$ cm^{-1} and ωx ranges from

https://doi.org/10.1021/acs.jpca.1c05025
J. Phys. Chem. A 2021, 125, 7185−7197

0 to 500 cm^{-1}, where 500 cm^{-1} is roughly the anharmonicity of the OH stretch in $H_7O_3^+$. For this part of the study, we obtain the ground state wave function using a discrete variable representation (DVR) based on an evenly spaced grid[40] consisting of 800 points in $\Delta r = r - r_e$ ranging from −1.00 to 3.00 a_0, or −0.529 to 1.59 Å. We then calculate the energy differences between the states with n = 1 or 2 and the ground state using the expressions provided in eqs 12−19.

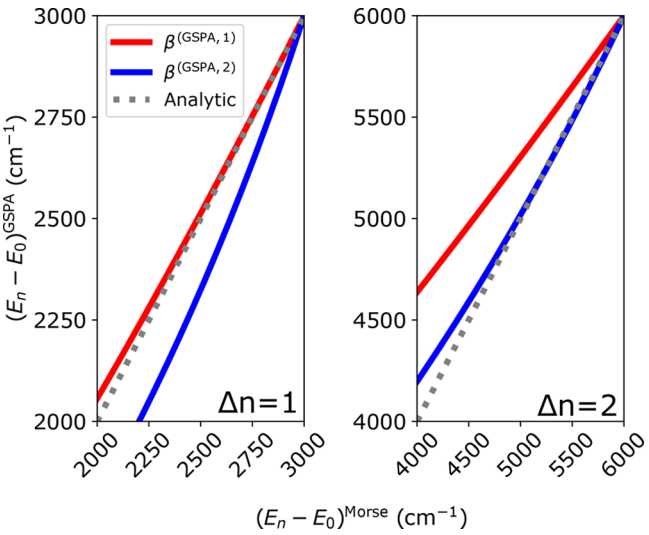

Figure 1. Comparison of the transition energies for Δn = 1 (left) and Δn = 2 (right) obtained using the GSPA approach with $\beta^{(GSPA,m)}$ defined in eqs 18 for m = 1 (red solid line) and 19 for m = 2 (blue solid line) to the expected values for Morse oscillators (gray dotted line) with harmonic frequencies of 3000 cm^{-1} and anharmonicities between 1 and 500 cm^{-1} (see eq 20).

In Figure 1, we compare the results of these calculations using $\beta^{(GSPA,1)}$ (red solid line) and $\beta^{(GSPA,2)}$ (blue solid line) to the energies evaluated using eq 25 (gray dotted line). The plot on the left shows results for the Δn = 1 transitions, while results for the Δn = 2 transitions are shown in the right panel. Consistent with earlier studies,[33] calculating the transition energy to the state with n = 1, using $\beta^{(GSPA,1)}$ in the expression for the kinetic energy provides more accurate excited state energies, and the percent error of the calculated transition energy is less than 3% over this range of anharmonicities. This is illustrated by the agreement between the solid red and dotted gray lines in the left panel of this figure. Using $\beta^{(GSPA,2)}$ (results shown with the blue solid line) to calculate the n = 1 energies yields much poorer agreement with the expected results (shown with the gray dotted line). When $\beta^{(GSPA,1)}$ is used to evaluate the transition energies to states with n = 2, the values are overestimated. This can be seen by comparing the results plotted with the red solid line and the gray dotted line in the right panel of this figure. On the other hand, if we use $\beta^{(GSPA,2)}$ (results shown with the blue solid line) to evaluate the energies of the Δn = 2 transitions, the error is smaller than 5% over a large range of anharmonicities. Based on these results, we will use the expressions for β provided in eqs 18 and 19 based on the value of Δn in the calculations described below.

Structure and Internal Coordinates of H_3O^+, $H_7O_3^+$, and $H_9O_4^+$. The GSPA approach is predicated on finding an appropriate set of internal coordinates as well as a reference structure for evaluating the Cartesian components of the dipole moment. The most important consideration in identifying a reference structure is that it is energetically accessible in the vibrational ground state. It should also reflect the symmetry of the vibrationally averaged structure of the system of interest.[41] In the present study, we are focusing on ions that can be characterized as hydronium bound to two or three water molecules. Based on previous studies,[25] as well as examining projections of the DMC probability amplitude, we choose for the reference structure one in which the hydronium core is planar, the oxygen atoms are in the same plane as the hydronium core, and the water molecules lie in planes that are perpendicular to the plane that contains the oxygen atoms. These reference structures are illustrated in the top panels of Figure 2. Once defined, we need a way to rotate an arbitrary structure to this reference structure. With the large amplitude umbrella motions of the hydrogen atoms in the hydronium core and the large amplitude rotations of the outer water molecules, we choose to base this on the coordinates of the oxygen atoms and use standard algorithms[42,43] to rotate arbitrary structures to the reference geometry.

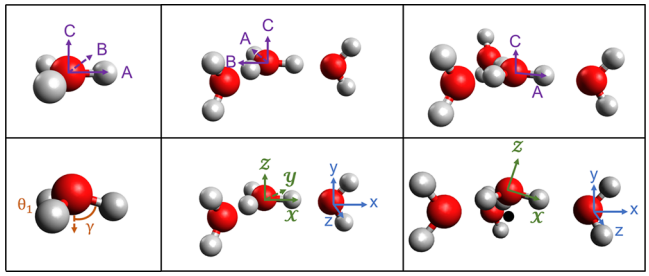

Figure 2. (Top) Reference structures for H_3O^+ (left), $H_7O_3^+$ (middle), and $H_9O_4^+$ (right) used in this study. The heavy atoms and the hydrogen atoms in the hydronium core are all coplanar. Additionally, in $H_7O_3^+$ and $H_9O_4^+$, the outer water molecules lie in planes that are perpendicular to the heavy atom plane. The purple A, B, and C axes are used to define the modified Eckart frame described in the text. (Bottom left) The umbrella coordinate (γ) and one of the HOH angles (θ_1) are defined for H_3O^+. (Bottom Middle and Right) The axis systems used to define the orientation of the outer water molecules (see text for details), are shown in green and blue. The black circle in the lower right panel shows the point in the plane containing the three outer oxygen atoms that is closest to the central oxygen atom, and is used in the definition of the $\mathcal{XZ}$ plane.

With the reference structure determined, we define internal coordinates. Since the GSPA approximation is based on a harmonic description of molecular vibrations, in selecting coordinates, we aim to identify ones for which the projections of Φ_0^2 onto the chosen coordinates are roughly Gaussian. This criterion is not always achievable, particularly for some of the large amplitude motions that correspond to the umbrella motion of the hydronium core and the hindered rotation of the outer water molecules. In addition, the coordinates are chosen such that we can construct symmetry adapted linear combinations of the coordinates that reflect the symmetry of the reference structure of the ion.

If we consider H_3O^+, three of the six internal coordinates are the three OH bond lengths. In the planar reference structure there is redundancy in the HOH angles. We use two linear combinations of these angles that transform as the E irreducible representation under the D_{3h} symmetry group, $2\theta_1 - \theta_2 - \theta_3$ and $\theta_2 - \theta_3$. The sixth coordinate, γ, is an umbrella coordinate, which is the angle between a vector

https://doi.org/10.1021/acs.jpca.1c05025
J. Phys. Chem. A 2021, 125, 7185−7197

Table 1. Calculated Vibrational Transition Energies of H_3O^+ (cm^{-1})

state	sym	assignment	GSPA	VSCF/VCI[a]	VPT2[b]
(0,0,0,0)	A_1'	ground state	0	0/38.6	0
(0,1,0,0)	E′	antisymmetric OH stretch	3535/3535	3545	3502
(1,0,0,0)	A_1'	symmetric OH stretch	3406	3416	3410
(0,0,1,0)	E′	H_3O^+ bend	1617/1617	1623	1625
(0,0,0,1)	A_2''	umbrella	151	573/945	734
(0,2,0,0)	A_1'		6983	6972	6879
(0,2,0,0)	E′		6998/7031	7068	6944
(2,0,0,0)	A_1'		6746	6748	6768
(0,0,2,0)	A_1'		3212	3211	3211
(0,0,2,0)	E′		3215/3233	3233	3236
(0,0,0,2)	A_1'		705	1462/2030	1290

[a]Based on HCB-4 potential.[38,39] [b]MP2/aug-cc-pVTZ.

shown in the lower panel of Figure 2 that has its origin at the oxygen atom and passes through the center of a triangle, which is defined by the vertices of unit vectors along each of the three OH bonds, and a second vector that lies along one of the OH bonds. This definition ensures that the value of the umbrella coordinate is independent of the OH bond that is used to define it.

Defining the coordinates for $H_7O_3^+$ and $H_9O_4^+$ requires an overall axis system (expressed as *A*, *B*, *C*, and shown in purple in the upper panels of Figure 2). To define these axes, we use a modified Eckart frame. In $H_7O_3^+$, this frame is based on the coordinates of the three oxygen atoms, while in $H_9O_4^+$ we use the three outer oxygen atoms to define the Eckart frame.[42,43] Once the reference structure has been rotated to a principle axis frame, with the origin of the axis system at the center of mass of the three oxygen atoms that are used to define this axis system, these three oxygen atoms all lie in the *AB*-plane. In $H_7O_3^+$, the central oxygen atom is on the *A*-axis, while in $H_9O_4^+$ one of the external oxygen atoms is on the *A*-axis. For $H_7O_3^+$, this is the same as the axis system that is used to define the components of the dipole moment surface, while for $H_9O_4^+$, the coordinate systems differs due to the exclusion of the fourth oxygen atom from the definition of the modified Eckart frame.

We then define the internal coordinates of the constituent water and hydronium molecules. Each outer water molecule is described by two OH bond lengths and one HOH angle. The three OH bonds in the hydronium core are described in terms of three spherical polar coordinates, with θ providing the angle between the OH bond and the *C*-axis, while ϕ provides the rotation of the OH vector off of the *A*-axis in the *AB* plane. For the free OH in the hydronium core in $H_7O_3^+$, we replace ϕ with ϕ', which is the difference between the two $H_{Free}OH_{Bound}$ angles, as ϕ becomes ill-defined when θ approaches 0° and 180°.

The orientations of the outer water molecules are each defined using three Euler angles. For both $H_7O_3^+$ and $H_9O_4^+$, the axes that describe the orientation (x, y, z) of the water molecules are defined with the *x*-axis pointing along the bisector of the two OH vectors, and the *z*-axis as the cross product between the two OH vectors. For $H_7O_3^+$, three Euler angles define the rotation between the axis system for the water molecule of interest (x, y, z) and one $(\mathcal{X}, \mathcal{Y}, \mathcal{Z})$ in which the OO vector from the central oxygen atom to the oxygen atom in the water molecule of interest lies along the $\mathcal{X}$-axis, and the third oxygen atom lies in the $\mathcal{XY}$ plane, with the direction of the $\mathcal{Z}$-axis being determined by the cross product of the OO vectors from the central to the outer oxygen atoms. In this way, the $\mathcal{Z}$-axis is the same for both water molecules, while the orientation of the $\mathcal{X}$ and $\mathcal{Y}$ axes is determined by which water molecule is being considered (see Figure 2). Likewise for $H_9O_4^+$, the three Euler angles relate the axis system for the water molecule of interest to an axis system where the $\mathcal{X}$-axis points along the OO vector from the central oxygen atom to the oxygen atom in the water molecule being considered. The $\mathcal{XZ}$ plane contains these two oxygen atoms as well as the point on the *AB* plane that is closest to the central oxygen atom. The $\mathcal{Y}$-axis is defined by $\mathcal{Z} \times \mathcal{X}$ (see Figure 2).

Finally, we use the OO distances and the OOO bending coordinate to describe the relative distances between the hydronium and the outer water molecules in $H_7O_3^+$. For $H_9O_4^+$, we use the three outer OO distances as well as the three Cartesian displacements of the center of mass of the hydroninum core based on the modified Eckart axis system described above. For the purposes of assignments, the *C*-axis is defined as the one that is perpendicular to the plane defined by the oxygen atoms.

Application to H_3O^+. As a test of the approximation to the expectation value of the kinetic energy described above, we apply the GSPA approach to the calculation of the transition energies in H_3O^+, where the results can be compared to the results of VSCF/VCI calculations by Huang et al. using the same potential surface.[38,39] We also compare to the results of VPT2 calculations. The VPT2 energies were obtained at the MP2/aug-cc-pVTZ level of theory/basis as implemented in Gaussian 16.[44]

The results of the calculations are reported in Table 1. Focusing on the states with one quantum of excitation in one of the vibrational modes, the states with excitation in the OH stretches or HOH bends obtained using the GSPA approach are in very good agreement with the results of VSCF/VCI calculations. In addition to reporting the excited state energy and assignment, we provide the symmetry of the excited state based on the D_{3d} reference structure. The energies that were calculated using the GSPA approximation reflect the expected degeneracies of the antisymmetric OH stretch and the HOH bend. While the five high-frequency vibrations are well-described by this approach, the frequency of the fundamental in the umbrella vibration is not in as good agreement with the VSCF/VCI values. Due to the double well character of the potential along the umbrella coordinate, the state with a node at the planar reference structure will correspond to the upper level of the ground-state tunneling doublet and not a proper first excited state in this vibration. The measured ground state

https://doi.org/10.1021/acs.jpca.1c05025
J. Phys. Chem. A 2021, 125, 7185−7197

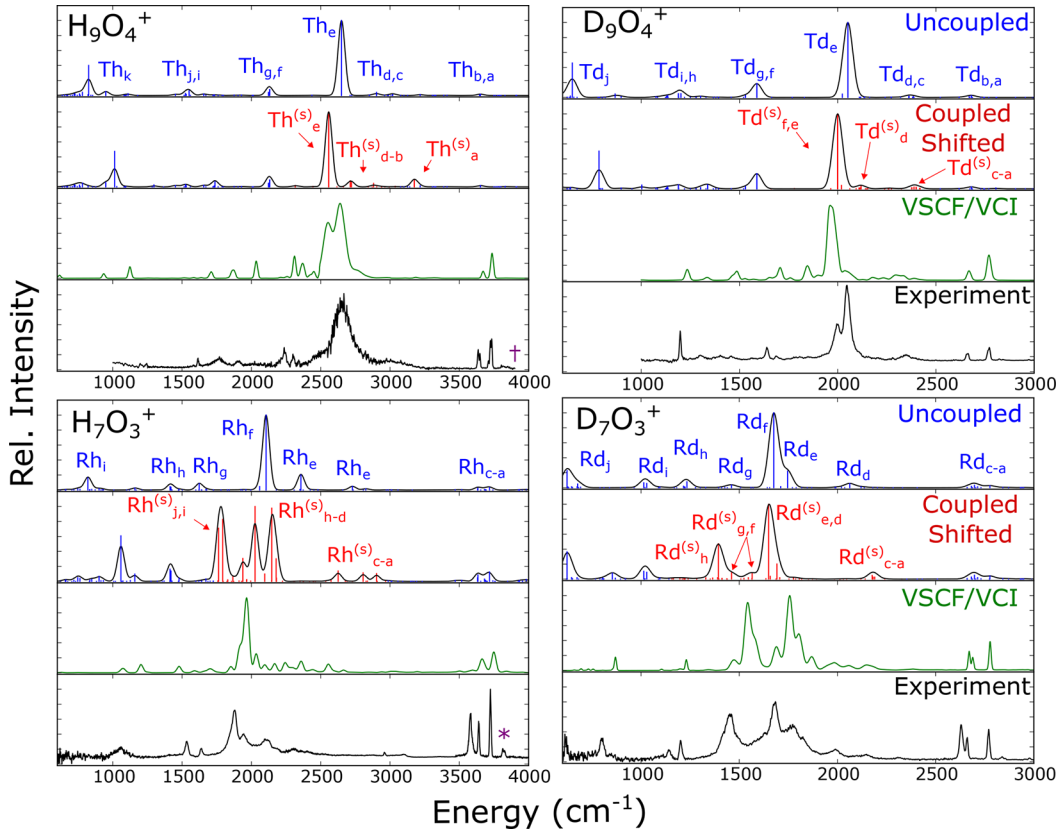

Figure 3. Comparison of the uncoupled (blue sticks), coupled and shifted (red sticks), VSCF/VCI[13,26] (green), and measured spectra[13,20] (black) of $H_9O_4^+$ (top left), $D_9O_4^+$ (top right) $H_7O_3^+$ (bottom left), and $D_7O_3^+$ (bottom right). In these spectra, the Th and Rh labels are used to denote transitions in $H_9O_4^+$ and $H_7O_3^+$, respectively, while Td and Rd are used to refer to peaks in the spectra of the deuterated forms of these ions. The purple * and † identify transitions in $H_7O_3^+$ and $H_9O_4^+$, which were assigned by the authors to combination transitions. Descriptions of the states accessed by labeled uncoupled transitions in the GSPA spectra are provided in Tables S4−S7, and the coupled shifted transitions are provided in Tables S8−S11.

tunneling splitting in H_3O^+ is 55 cm^{-1},[45] and calculations based on this potential yield a ground state tunneling splitting of 38.6 cm^{-1}.[39]

When we compare the calculated energy of the state with two quanta of excitation in the umbrella vibration to that obtained from a VPT2 calculation, we find that the n = 2 energy from the GSPA calculation is close to the calculated energy of the state with one quantum of excitation. It is also close to the average energy of the tunneling split n = 1 states obtained from the VSCF/VCI calculation (573 and 945 cm^{-1}). If we recalculate the energy of the n = 1 state using $\beta^{(GSPA,2)}$ in the evaluation of the kinetic contribution, the calculated energy is 556 cm^{-1}, which is 17 cm^{-1} smaller than the energy of the lower energy n = 1 state, based on the VSCF/VCI calculation. Clearly, the umbrella vibration is a challenging one to describe using the GSPA approach, which is based on a harmonic treatment of molecular vibrations about a planar reference structure, and we are encouraged by the fact that we can obtain a reasonably good description of this motion in H_3O^+.

When we compare the energies of the states with two quanta of excitation to those obtained using VPT2 and VSCF/VCI energies, the agreement remains good for all but the umbrella vibration. In the case of the antisymmetric stretch and bend, which have E′ symmetry, the states with n = 2 will correspond to three transitions, two of which are degenerate, and one with A′ symmetry. The energies of the overtones in the OH stretch and the HOH bend with A′ symmetry are in very good agreement with the VSCF/VCI results, further validating the expressions for $\beta^{(2,GSPA)}$ in eq 19. On the other hand, for the pair of states with E′ symmetry, there is a notable difference between the two calculated energies, with the higher energy one being in better agreement with the VSCF/VCI results. The loss of degeneracy for the overtones with E′ symmetry reflects, in part, the fact that the first value is treated as a state with two quanta in one of the two degenerate vibrations, while the second value is obtained by putting one quantum in each of the two degenerate vibrations. Based on these comparisons, we find that the GSPA technique also does a good job of describing the overtones of the stretches and bends in hydronium, although some care should be taken in handling degenerate vibrations. Additionally, the good agreement with VSCF/VCI results for states with one quantum in each of two vibrations validates our definition of the energies of these excited states.

Examining the Vibrational Spectrum of $H_7O_3^+$ and $H_9O_4^+$. The richest region of the spectra for $H_7O_3^+$ and $H_9O_4^+$ is the region that contains transitions to n = 1 levels of the OH stretches and the HOH bend (i.e., the 1000−4000 cm^{-1} region). As can be seen in the black traces in Figure 3, this region is characterized by intense features near the expected location of the fundamental in the shared proton stretch, which is near 2100 cm^{-1} in $H_7O_3^+$ and 2600 cm^{-1} in $H_9O_4^+$. There are several narrow peaks near 3500 cm^{-1}, where the OH stretch fundamental in water is expected, as well as a series of

https://doi.org/10.1021/acs.jpca.1c05025
J. Phys. Chem. A 2021, 125, 7185−7197

less intense peaks at lower frequency. Except for the region near the transition to the n = 1 state in the shared proton stretch, the measured spectra of $H_7O_3^+$ and $H_9O_4^+$ appear to be very similar to each other. The primary difference between the spectra for $H_7O_3^+$ and $D_7O_3^+$ and between $H_9O_4^+$ and $D_9O_4^+$ can be accounted for by the factor of $\sqrt{2}$ difference between frequencies of the OH stretch and HOH bend vibrations involving deuterium compared to those involving hydrogen. The results of the GSPA approximation are shown with blue sticks in the upper panel for each ion in Figure 3. The peaks in the calculated spectra are labeled, and the corresponding energies and assignments are provided in Tables S4−S7. The Th and Rh labels are used to denote transitions in $H_9O_4^+$ and $H_7O_3^+$, respectively, while Td and Rd are used to refer to peaks in the spectra of the deuterated forms of these ions. For comparison, we also provide the VSCF/VCI spectra, which were reported by Yu and Bowman, green traces in Figure 3.[13,26] Overall, the spectra calculated using the GSPA approach, shown in red, are in good agreement with both the spectra calculated using the VSCF/VCI with the same potential surface and the measured spectra.

Table 2. Calculated GSPA, VSCF/VCI and Measured Transitions in the Outer OH Stretch Region for $H_7O_3^+$ (cm^{-1})

GSPA	VSCF/VCI[a]	measured[a]	assignment[a]
3769, 3772, 3786, 3790	–	3814, 3828	H_2O antisym. stretch + H_2O torsion
3761	3748	3726	outer water OH antisym. H_2O stretch
3632	3658	3640	outer water OH sym. H_2O stretch
3634	3664	3580	hydronium free OH stretch

[a]Reference 13.

Free OH Stretching Vibrations. The higher frequency end of this region of the measured spectrum, shown in black traces in Figure 3, is characterized by a series of narrow peaks. In earlier studies, these peaks were assigned to transitions to states with one quantum in the OH or OD stretches in the flanking water molecules or the free OH stretch on the hydronium core in $H_7O_3^+$. To facilitate the comparison between calculated and measured spectra, the calculated frequencies and intensities of these transitions are also reported in Tables 2 and 3. As can be seen, the GSPA approach generally provides energies that are within 30 cm^{-1} of both the measured values and those obtained from VSCF/VCI calculations by Yu and Bowman.[13,20] These differences are consistent with the differences between the GSPA approach and the results of MCTDH calculations for $H_5O_2^+$,[18,34] the differences between the GSPA and VSCF/VCI results for $H_3O_2^-$,[33] and the comparisons for H_3O^+. The only exception is the transition in $H_7O_3^+$ that has been assigned to the free OH stretch in the hydronium core. Both the VSCF/VCI and GSPA approaches show larger deviations from the measured position of this transition compared to the other OH stretch transitions in this region of the spectrum. The measured spectrum of $H_7O_3^+$ is obtained by monitoring the loss of the tag molecule (M) from M·$H_7O_3^+$, where the tag has been shown to attach to the free hydrogen atom in the hydronium core. Recent experimental studies showed that this is the vibration whose frequency is most sensitive to the strength of the interaction with the tag. VPT2 calculations, which were performed as part of that study, showed a shift in the anharmonic frequency of this OH stretch of 90 cm^{-1} when it is bound to D_2 and a 50 cm^{-1} shift when the OD bond in $D_7O_3^+$ is bound to D_2.[19]

Table 3. Calculated GSPA, VSCF/VCI and Measured Transitions in the Outer OH Stretch Region for $H_9O_4^+$ (cm^{-1})

GSPA	VSCF/VCI[a]	measured[a]	assignment[a]
3757, 3759, 3759, 3769, 3775, 3782, 3786, 3790, 3800	–	3823, 3803	H_2O antisym. stretch + H_2O torsion
3733, 3762	3734	3733	outer water OH antisym. H_2O stretch
–	–	3724	tagged outer water OH antisym. H_2O stretch
3652, 3694	3670	3648	outer water OH sym. H_2O stretch
–	–	3636	tagged outer water OH sym. H_2O stretch

[a]Reference 20.

Further examination of the fundamental frequencies and intensities of the OH stretching vibrations in $H_7O_3^+$ and $H_9O_4^+$, reported in Tables S1 and S2, shows that the fundamental transition of the antisymmetric stretch of the water molecules does not carry any intensity, and the fundamental transition of the in-phase combination of the OH symmetric stretches in $H_9O_4^+$ is also dark. The lack of intensity in the fundamental in the symmetric stretch can be anticipated from the average symmetry of the ion. On the other hand, the lack of intensity of the antisymmetric water OH stretch is somewhat surprising, and was not anticipated by previous VSCF/VCI studies.[13,20,22,26] Further consideration of this vibration shows that in simpler ion−water complexes, e.g. Li^+OH_2, in which the cation binds along the C_2 axis of the water molecule, the antisymmetric OH stretch is associated with ΔK = 1, or a change in the number of quanta of excitation in the motion associated with rotation of the water molecule about its symmetry axis.[46] Depending on the size of the barrier for internal rotation of the flanking water molecules, these transitions will either access a ΔK = 1 transition or access the upper level in the tunneling doublet for the state with one quantum of excitation in both the OH stretch and the rotation of the water molecule about its symmetry axis. Previous analyses of the ground state probability amplitudes for $H_7O_3^+$ and $H_9O_4^+$ showed large amplitude rotation of the flanking water molecules about this axis, which would be consistent with these levels being energetically split by a small tunneling splitting.[25] This rotation was not included in VSCF/VCI calculations, which is why these calculations anticipated intensity in the Δn_{OH} = 1 transitions involving the outer water molecules. While this tunneling splitting is not resolved in the experiment, the spectra of both $H_7O_3^+$ and $H_9O_4^+$ contain features which have been assigned to excitation to states that have a quantum of excitation in both the antisymmetric OH stretch and in this torsion motion.[12] These transitions are indicated with the purple * and † in the measured spectra in Figure 3, and we report the calculated energies for these transitions based on the GSPA approach in Tables 2 and 3.

https://doi.org/10.1021/acs.jpca.1c05025
J. Phys. Chem. A 2021, 125, 7185−7197

Umbrella Vibration. The fundamental in the umbrella motion lies at the other end of this spectral range. As noted for hydronium, the large amplitude nature of this mode, which samples a double well potential with a small barrier, makes it a challenging one for the GSPA approach. For both $H_7O_3^+$ and $H_9O_4^+$, the frequency of this vibration calculated using the GSPA approach is roughly 200 cm^{-1} smaller than the observed transition frequency, which is near 1000 cm^{-1} for both of these ions.[13,14,20] The underestimation of the frequency of this vibration is consistent with our findings for H_3O^+. Like H_3O^+, the umbrella motions in $H_7O_3^+$ and $H_9O_4^+$ both sample a double-well potential, and for both ions the projection of the ground state probability amplitude onto this coordinate is bimodal.[25] This makes the GSPA approach, which is based on properties of harmonic oscillators, less effective for this vibration. The underestimation of the frequency of the umbrella mode will also affect the energies of states that have one quantum of excitation in the umbrella along with one quantum of excitation of one of the higher frequency vibrations. To account for this, in the spectra that are identified as "coupled shifted" in Figure 3, we have shifted the transition energies of the states that involve the umbrella mode by the error in the calculated transition energy to the $n = 1$ level prior to diagonalization of the Hamiltonian matrix. The values of these shifts are provided in Table S3. Because the frequency of the umbrella in $D_9O_4^+$ has not been reported, the shift for this ion was evaluated based on the shifts for the other three species. A comparison of the calculated GSPA spectrum with and without this shift is provided in Figure S1.

Shared Proton Stretch Vibration. The most interesting region of the spectrum includes the fundamental in the shared proton stretch. In the absence of state mixing, the GSPA energies of the $\Delta n = 1$ transitions in the shared proton stretch vibration for $H_9O_4^+$ and $D_9O_4^+$ (Th_e and Td_e) are in excellent agreement with experiment. In the case of $H_7O_3^+$ and $D_7O_3^+$, the energies of the $\Delta n = 1$ transition in the shared proton stretch (Rh_f and Rd_f) are close to the centroids of the experimental signal in the shared proton region.[19] While the agreement is generally very good, the measured peaks in $H_7O_3^+$, $D_7O_3^+$, $H_9O_4^+$, and $D_9O_4^+$ in this region have been attributed to states of mixed character. The states that are nearly degenerate to the shared proton stretch undergo intensity borrowing, leading to the observed broad and structured features seen in the experimental traces shown in Figure 3.[13,19,20,24,26]

To account for this state mixing, we explore how the spectra in the region of the fundamental in the shared proton stretch changes if we introduce couplings among the $n = 1$ states in the shared proton stretch and energetically nearby zero-order states. We can then examine the contributions from the zero-order vibrational states to the excited state of interest by calculating the coefficients (C_n) of the eigenvectors of the reduced dimensional Hamiltonian matrix obtained from solving the generalized eigenvalue problem (eq 24). The resulting spectra, obtained by considering states with two or fewer quanta of excitation and with energies that are within 600 cm^{-1} of the anharmonic frequency of the shared proton stretch in $H_7O_3^+$ and $D_7O_3^+$ and within 400 cm^{-1} of the shared proton stretch in $H_9O_4^+$ and $D_9O_4^+$, are shown with red sticks in the middle panels of Figure 3. Transitions to states that were not included in this analysis are shown with blue sticks in these panels. The transitions are identified with the (s) superscript to reflect the fact that we have introduced a shift in the frequency of the umbrella vibration prior to diagonalizing the Hamiltonian matrix. The associated frequency and decomposition in terms of zero-order states are provided in Tables S8−S11. The assignments of the transitions in the uncoupled region of the spectrum are provided in Tables S4−S7.

The small basis representation of the Hamiltonian yields a spectrum that is in good agreement with both the measured spectrum and the spectrum obtained from a VSCF/VCI calculation, which employed a substantially larger basis. The use of a small basis allows us to decompose the contributions to the various features in the spectrum. In fact, the state-mixing treatment used in the GSPA approach is similar to the approach that is used to account for near-degeneracies in vibrational perturbation theory calculations. In an earlier study, we used VPT2 to explore mode mixing in $H_7O_3^+$, $D_7O_3^+$ and $H_9O_4^+$, where the VPT2 was based on an expansion of the Hamiltonian in internal coordinates.[25,27] The results of that study are summarized in Tables S16−S18 to aid in the discussion that follows.

We begin by considering the results of the GSPA calculations of the spectra for $H_9O_4^+$ and $D_9O_4^+$. For these ions, the introduction of state mixing leads to subtle changes in the spectral envelope. The most significant change is that the peak that corresponds to the fundamental in the antisymmetric shared proton stretch is shifted to the red in both systems. These shifts result from mixing of the states with one quantum of excitation in the shared proton stretch and states with one quantum of excitation in both the shared proton stretch and the OO stretch. While these shifts lead to poorer agreement with the measured spectrum, the peak that is assigned to the transition to the state with one quantum of excitation in the shared proton stretch in $D_9O_4^+$ becomes closer to the position of the corresponding peak in the VSCF/VCI spectrum.

In addition, the transitions identified as $Th_{a\text{-}d}^{(s)}$ and $Td_{a\text{-}d}^{(s)}$ gain intensity and better reproduce the corresponding features in the measured spectrum of $H_9O_4^+$ near 3000 cm^{-1} and the feature near 2350 cm^{-1} in calculated spectrum for $D_9O_4^+$. These peaks have been assigned to transitions to states with one quantum of excitation in the shared proton stretch and one quantum in the corresponding OO stretch,[20] which is consistent with the decomposition of the GSPA states that are accessed by these transition (see Tables S8 and S9).

While the main features in this spectral region are reproduced by the coupled GSPA calculation, the widths of some of the peaks are not. The breadth of the peak near 2600 cm^{-1} in $H_9O_4^+$ suggests couplings to energetically proximal states, many of which involve more than two quanta of excitation. The large density of vibrational states at this energy makes it impossible to reproduce the breadth of this feature using a method that focuses on states with only one or two quanta of vibrational excitation. For this reason, as we consider the results of the GSPA calculations, we focus on the position of this transition, rather than the width of the feature. As noted, the position of these features are generally in very good agreement with previous VSCF/VCI calculations despite the much smaller basis used in the GSPA approach.

We next turn our attention to $H_7O_3^+$ and $D_7O_3^+$. By comparison to the corresponding spectra for $H_9O_4^+$ and $D_9O_4^+$, the region of the spectrum that has been assigned to transitions to the $n = 1$ state in the shared proton stretch in $H_7O_3^+$ and $D_7O_3^+$ contains significantly more structure. This has been attributed to couplings between this state and states with two quanta of excitation in lower frequency modes.[13,19,24]

https://doi.org/10.1021/acs.jpca.1c05025
J. Phys. Chem. A 2021, 125, 7185−7197

In contrast to the breadth of the shared proton stretch feature in the spectrum for $H_9O_4^+$, this is an effect that should be accessible by the GSPA approach.

When we introduce state mixing in the GSPA calculation, the resulting spectra undergo dramatic changes in the region where the transition to the state with one quantum of excitation in the shared proton stretch had been in the uncoupled spectrum (Rh_f and Rd_f in the blue trace in Figure 3). Additionally the band profiles for $H_7O_3^+$ and $D_7O_3^+$ have qualitatively different shapes. In the case of $H_7O_3^+$, the intensity spans from 1760 to 2180 cm^{-1}, while it spans from 1400 to 1700 cm^{-1} in $D_7O_3^+$. Qualitatively, this increase in the number of transitions that carry significant intensity correlates to the features in the measured and VSCF/VCI spectra. One of the advantages of the GSPA approach is that it employs a small basis, making the interpretation of the zero-order states that make up the states that are accessed in these transitions straightforward to identify, and these decompositions for $H_7O_3^+$ and $D_7O_3^+$ are summarized in Tables S10 and S11. Examination of these results shows that the most intense features of the calculated GSPA spectrum are composed of states with two quanta of excitation in combinations of the OO stretch, H_3O^+ HOH bends, the umbrella mode, and the hindered rotation of the hydronium core.

Intuitively, the transfer of a proton from hydronium to an acceptor water molecule requires deformations of the water cluster. This in turn involves motions such as the OO stretch as well as the HOH angles in both hydronium and water.[14,20,25,47] Likewise, motions that break the hydrogen bond network through rotation of the hydronium core affect the potential energy surface along the shared proton stretch coordinate. These changes in the potential landscape with proton transfer result in the large couplings between the excited states of $H_7O_3^+$ that involve these motions. These large couplings provide the source of the large changes in the spectra when coupling is introduced in the GSPA calculation. The decomposition of the eigenvectors of the degenerate VPT2 calculations,[25,27] which are provided in Tables S16 and S17, identify similar mixing patterns to those identified from the GSPA approach.

Turning our attention to the comparison of both the measured and calculated spectra of $H_7O_3^+$ with $D_7O_3^+$, we note significant differences. The change in the structure of the spectrum upon deuteration of $H_7O_3^+$ has been discussed previously,[13,19,24] and it reflects the fact that the energies of the zero-order states that are strongly coupled to the shared proton stretch are each shifted by different amounts. Additionally, the smaller amplitude OD vibrations, compared to the OH vibrations, leads to smaller couplings between the various zero-order states when we allow these states to mix. Similar considerations explain the large difference in the structure of the most intense features in the spectra of $H_9O_4^+$ and $H_7O_3^+$. The couplings that result in the more structured feature in $H_7O_3^+$ and $D_7O_3^+$ are also present in $H_9O_4^+$ and $D_9O_4^+$. The smaller amplitude motion of the shared proton stretch in $H_9O_4^+$ decreases the magnitude of these couplings. More importantly, though, the higher frequency of the shared proton stretch vibration in $H_9O_4^+$ brings it out of resonance with the states with two quanta of excitation in lower frequency vibrations that contribute to the shared proton stretch feature in $H_7O_3^+$.

Low Frequency Vibrations. Finally, we consider the low frequency (200−800 cm^{-1}) region of the spectrum reported by Asmis and co-workers.[15] This region of the spectrum provides direct access to the motions that are mixed with the shared proton stretch in the higher energy regions of the spectrum. In the GSPA approach the coordinates are developed from the ground state wave function, and as a result, the calculated energies capture the anharmonicity of the potential. This allows us to obtain a good description of this spectral region, which is difficult to study using VPT2 and other approaches that are based on a normal mode Hamiltonian.

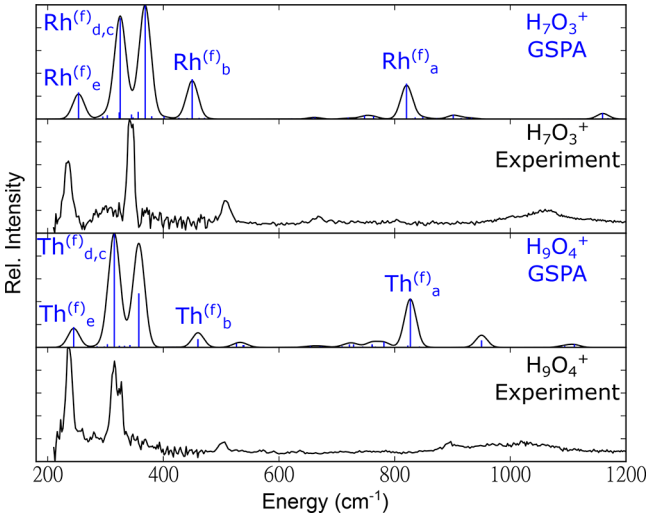

Figure 4. Calculated uncoupled GSPA spectrum (blue sticks) compared with experiment[15] (black) for $H_7O_3^+$ and $H_9O_4^+$. The assignments of the labeled transitions are provided in Table S19. In these spectra, the $Th^{(f)}$ and $Rh^{(f)}$ labels are used to denote far-IR transitions in $H_9O_4^+$ and $H_7O_3^+$, respectively.

The calculated and measured spectra for $H_7O_3^+$ and $H_9O_4^+$ are shown in blue and black, respectively, in Figure 4, where we introduce a (f) superscript to the peak labels to indicate that these transitions lie in the far-IR region of the spectrum.. In the measured spectrum, the low frequency regions of $H_7O_3^+$ and $H_9O_4^+$ contain peaks at similar frequencies. We attribute many of the features of both spectra to analogous low frequency vibrational motions (see Table S19). There are two intense features in this region of the $H_7O_3^+$ and $H_9O_4^+$ spectrum. Based on the GSPA approach, the lower energy feature is assigned to the fundamental transition in the in-phase outer water rock ($Rh_d^{(f)}$ and $Th_d^{(f)}$) for both $H_7O_3^+$ and $H_9O_4^+$. The higher energy feature is assigned to the antisymmetric OO stretch in $H_7O_3^+$ and the two degenerate antisymmetric OO stretches in $H_9O_4^+$ ($Rh_c^{(f)}$ and $Th_c^{(f)}$).

Based on quasiclassical calculations of $H_7O_3^+$, the lower energy feature at 234 cm^{-1} was assigned to be the outer water wag, and the higher energy feature at 344 cm^{-1} was assigned to be the symmetric OO stretch. For $H_9O_4^+$, the lower energy feature was assigned to the outer water wag, and the higher energy feature was assigned to both the symmetric and antisymmetric OO stretch. The peak at approximately 500 cm^{-1}, which in previous work was assigned as a combination of low frequency modes,[15] is assigned using the GSPA approach as an outer water wag overtone transition in $H_7O_3^+$ and two degenerate outer water wag combinations in $H_9O_4^+$ ($Rh_b^{(f)}$ and $Th_b^{(f)}$). The good agreement between the GSPA results and the measured spectra in this region illustrates the power of the GSPA approach for describing the low-energy region of the

https://doi.org/10.1021/acs.jpca.1c05025
J. Phys. Chem. A 2021, 125, 7185−7197

spectra where the use of curvilinear coordinates is essential, while the low density of vibrational states results in little mixing among the carefully constructed zero-order states developed in this approach.

CONCLUSIONS

In this work, we extended the previously developed GSPA approach[33,34] to allow for more accurate descriptions of the energies of states with two quanta of excitation, provided better descriptions of coordinates, and introduced coupling between zero order states. This allowed us to exploit the rich structural and physical information contained in the DMC ground state probability amplitude of $H_7O_3^+$ and $H_9O_4^+$, as well as their deuterated analogs, to develop a compact basis set that can be used to calculate the spectra for these ions.

In the absence of state mixing, the GSPA approach allows us to assign many of the features in the spectra of these ions. State mixing becomes essential to explain the region of the spectrum near the $\Delta n = 1$ transition in the shared proton stretch. By allowing states with up to two quanta of excitation to mix, we obtain spectra that are in generally good agreement with the measured spectra for $H_7O_3^+$ and $D_7O_3^+$. While there are clear differences between the measured and calculated spectra in the region of the transition to the $n = 1$ state of the shared proton stretch, the agreement of the measured spectra with the spectra obtained using the GSPA approach and VSCF/VCI calculations is similar. The deviations are a reflection of the sensitivity of both calculations of these spectral regions to subtle details in the potential and approximations made in both calculations.

The power of the GSPA approach comes in the ability to use a small basis through systematic and careful choice of vibrational coordinates and basis functions. These choices are informed by the fully anharmonic ground state wave function, which has been obtained using DMC. While aspects of the calculation and the basis that is used are similar to some aspects of VPT2 calculations, the GSPA approach has the advantage that it does not suffer from the singularities that plague VPT2 calculations, particularly in systems like $H_7O_3^+$ and $H_9O_4^+$ that contain low-frequency, large-amplitude vibrations. Furthermore, the method relies on the ability to calculate the potential energy and dipole functions with sufficient accuracy for spectral evaluation and the ability to construct a set of internal coordinates as a basis for these calculations. While the availability of a potential often limits the types of systems that can be explored with the GSPA approach, we have recently expanded our DMC calculations to allow us to utilize direct evaluation of electronic energies.[48]

ASSOCIATED CONTENT

Supporting Information

The Supporting Information is available free of charge at https://pubs.acs.org/doi/10.1021/acs.jpca.1c05025.

Numerical details; description of coordinate labels for $H_7O_3^+$ and $H_9O_4^+$; axes used to define the modified Eckart frame for all systems; comparison of uncoupled, coupled, and coupled shifted GSPA spectra for all systems; state assignments for the GSPA calculation for all systems; uncoupled GSPA assignments for the shared proton stretch region for all systems; shifts applied to the states involving the umbrella mode for all systems; shifted, coupled GSPA assignments for the shared proton stretch region for all systems; coupled GSPA assignments for the shared proton stretch region for all systems; eigenvectors of degenerate VPT2 mixed states for intense features in the shared proton stretch region of $H_7O_3^+$, $D_7O_3^+$, and $H_9O_4^+$; and uncoupled GSPA assignments for the low frequency region of $H_7O_3^+$ and $H_9O_4^+$ (PDF)

AUTHOR INFORMATION

Corresponding Author

Anne B. McCoy − *Department of Chemistry, University of Washington, Seattle, Washington 98195, United States;* orcid.org/0000-0001-6851-6634; Phone: 206-543-7464; Email: abmccoy@uw.edu

Authors

Ryan J. DiRisio − *Department of Chemistry, University of Washington, Seattle, Washington 98195, United States;* orcid.org/0000-0003-1272-0112

Jacob M. Finney − *Department of Chemistry, University of Washington, Seattle, Washington 98195, United States*

Laura C. Dzugan − *Department of Chemistry, University of Washington, Seattle, Washington 98195, United States*

Lindsey R. Madison − *Department of Chemistry, Colby College, Waterville, Maine 04901, United States;* orcid.org/0000-0002-3947-8357

Complete contact information is available at: https://pubs.acs.org/10.1021/acs.jpca.1c05025

Notes

The authors declare no competing financial interest.

ACKNOWLEDGMENTS

Support from the Chemistry Division of the National Science Foundation (CHE-1856125) is gratefully acknowledged. Parts of this work were performed using the Ilahie cluster, which was purchased using funds from a MRI grant from the National Science Foundation (CHE-1624430). This work was also facilitated through the use of advanced computational, storage, and networking infrastructure provided by the Hyak supercomputer system and funded by the STF at the University of Washington. Finally, we thank Professors Mark Johnson and Knut Asmis for sharing the spectral traces shown in black in Figure 3 and 4, respectively. We also thank Dr. Qi Yu for providing the VSCF/VCI spectra shown in green in Figure 3.

REFERENCES

(1) Thämer, M.; De Marco, L.; Ramasesha, K.; Mandal, A.; Tokmakoff, A. Ultrafast 2D IR Spectroscopy of the Excess Proton in Liquid Water. *Science* **2015**, *350*, 78−82.

(2) Fournier, J. A.; Carpenter, W. B.; Lewis, N. H. C.; Tokmakoff, A. Broadband 2D IR Spectroscopy Reveals Dominant Asymmetric $H_5O_2^+$Proton Hydration Structures in Acid Solutions. *Nat. Chem.* **2018**, *10*, 932−937.

(3) Schaefer, J.; Backus, E. H. G.; Nagata, Y.; Bonn, M. Both Inter- and Intramolecular Coupling of O−H Groups Determine the Vibrational Response of the Water/Air Interface. *J. Phys. Chem. Lett.* **2016**, *7*, 4591−4595.

(4) Sovago, M.; Campen, R. K.; Wurpel, G. W. H.; Müller, M.; Bakker, H. J.; Bonn, M. Vibrational Response of Hydrogen-Bonded Interfacial Water is Dominated by Intramolecular Coupling. *Phys. Rev. Lett.* **2008**, *100*, 173901.

(5) Inoue, K.-i.; Ishiyama, T.; Nihonyanagi, S.; Yamaguchi, S.; Morita, A.; Tahara, T. Efficient Spectral Diffusion at the Air/Water

Interface Revealed by Femtosecond Time-Resolved Heterodyne-Detected Vibrational Sum Frequency Generation Spectroscopy. *J. Phys. Chem. Lett.* **2016**, *7*, 1811−1815.
(6) Verma, D.; Erukala, S.; Vilesov, A. F. Infrared Spectroscopy of Water and Zundel Cations in Helium Nanodroplets. *J. Phys. Chem. A* **2020**, *124*, 6207−6213.
(7) Sofronov, O. O.; Bakker, H. J. Nature of Hydrated Proton Vibrations Revealed by Nonlinear Spectroscopy of Acid Water Nanodroplets. *Phys. Chem. Chem. Phys.* **2020**, *22*, 21334−21339.
(8) Okumura, M.; Yeh, L. I.; Myers, J. D.; Lee, Y. T. Infrared Spectra of the Cluster Ions $H_7O_3^+ \cdot H_2$and.$H_9O_4^+ \cdot H_2$. *J. Chem. Phys.* **1986**, *85*, 2328−2329.
(9) Yeh, L. I.; Okumura, M.; Myers, J. D.; Price, J. M.; Lee, Y. T. Vibrational Spectroscopy of the Hydrated Hydronium Cluster Ions $H_3O^+ \cdot (H_2O)_n$ (n = 1, 2, 3). *J. Chem. Phys.* **1989**, *91*, 7319−7330.
(10) Headrick, J. M.; Diken, E. G.; Walters, R. S.; Hammer, N. I.; Christie, R. A.; Cui, J.; Myshakin, E. M.; Duncan, M. A.; Johnson, M. A.; Jordan, K. D. Spectral Signatures of Hydrated Proton Vibrations in Water Clusters. *Science* **2005**, *308*, 1765−1769.
(11) Yu, Q.; Carpenter, W. B.; Lewis, N. H. C.; Tokmakoff, A.; Bowman, J. M. High-Level VSCF/VCI Calculations Decode the Vibrational Spectrum of the Aqueous Proton. *J. Phys. Chem. B* **2019**, *123*, 7214−7224.
(12) Douberly, G. E.; Walters, R. S.; Cui, J.; Jordan, K. D.; Duncan, M. A. Infrared Spectroscopy of Small Protonated Water Clusters, $H^+(H_2O)_n$ (n = 2 - 5): Isomers, Argon Tagging, and Deuteration. *J. Phys. Chem. A* **2010**, *114*, 4570−4579.
(13) Duong, C. H.; Gorlova, O.; Yang, N.; Kelleher, P. J.; Johnson, M. A.; McCoy, A. B.; Yu, Q.; Bowman, J. M. Disentangling the Complex Vibrational Spectrum of the Protonated Water Trimer, $H^+(H_2O)_3$, with Two-Color IR-IR Photodissociation of the Bare Ion and Anharmonic VSCF/VCI Theory. *J. Phys. Chem. Lett.* **2017**, *8*, 3782−3789.
(14) Wolke, C. T.; Fournier, J. A.; Dzugan, L. C.; Fagiani, M. R.; Odbadrakh, T. T.; Knorke, H.; Jordan, K. D.; McCoy, A. B.; Asmis, K. R.; Johnson, M. A. Spectroscopic Snapshots of the Proton-Transfer Mechanism in Water. *Science* **2016**, *354*, 1131−1135.
(15) Esser, T. K.; Knorke, H.; Asmis, K. R.; Schöllkopf, W.; Yu, Q.; Qu, C.; Bowman, J. M.; Kaledin, M. Deconstructing Prominent Bands in the Terahertz Spectra of $H_7O_3^+$and:$H_9O_4^+$ Intermolecular Modes in Eigen Clusters. *J. Phys. Chem. Lett.* **2018**, *9*, 798−803.
(16) Huang, X.; Cho, H. M.; Carter, S.; Ojamäe, L.; Bowman, J. M.; Singer, S. J. Full Dimensional Quantum Calculations of Vibrational Energies of $H_5O_2^+$. *J. Phys. Chem. A* **2003**, *107*, 7142−7151.
(17) Yu, Q.; Bowman, J. M. Ab Initio Potential for $H_3O^+ \rightarrow H^+ + H_2O$: A Step to a Many-Body Representation of the Hydrated Proton? *J. Chem. Theory Comput.* **2016**, *12*, 5284−5292.
(18) Vendrell, O.; Gatti, F.; Meyer, H.-D. Full Dimensional (15-Dimensional) Quantum-Dynamical Simulation of the Protonated Water Dimer. II. Infrared Spectrum and Vibrational Dynamics. *J. Chem. Phys.* **2007**, *127*, 184303−1−10.
(19) Duong, C. H.; Yang, N.; Johnson, M. A.; DiRisio, R. J.; McCoy, A. B.; Yu, Q.; Bowman, J. M. Disentangling the Complex Vibrational Mechanics of the Protonated Water Trimer by Rational Control of Its Hydrogen Bonds. *J. Phys. Chem. A* **2019**, *123*, 7965−7972.
(20) Duong, C. H.; Yang, N.; Kelleher, P. J.; Johnson, M. A.; DiRisio, R. J.; McCoy, A. B.; Yu, Q.; Bowman, J. M.; Henderson, B. V.; Jordan, K. D. Tag-Free and Isotopomer-Selective Vibrational Spectroscopy of the Cryogenically Cooled $H_9O_4^+$ Cation with Two-Color, IR-IR Double-Resonance Photoexcitation: Isolating the Spectral Signature of a Single OH Group in the Hydronium Ion Core. *J. Phys. Chem. A* **2018**, *122*, 9275−9284.
(21) McDonald, D. C.; Wagner, J. P.; McCoy, A. B.; Duncan, M. A. Near-Infrared Spectroscopy and Anharmonic Theory of Protonated Water Clusters: Higher Elevations in the Hydrogen Bonding Landscape. *J. Phys. Chem. Lett.* **2018**, *9*, 5664−5671.
(22) Yu, Q.; Bowman, J. M. High-Level Quantum Calculations of the IR Spectra of the Eigen, Zundel, and Ring Isomers of $H^+(H_2O)_4$ Find a Single Match to Experiment. *J. Am. Chem. Soc.* **2017**, *139*, 10984−10987.
(23) Yu, Q.; Bowman, J. M. Classical, Thermostated Ring Polymer, and Quantum VSCF/VCI Calculations of IR Spectra of $H_7O_3^+$ and $H_9O_4^+$ (Eigen) and Comparison with Experiment. *J. Phys. Chem. A* **2019**, *123*, 1399−1409.
(24) Samala, N. R.; Agmon, N. The Protonated Water Trimer and its Giant Fermi Resonances. *Chem. Phys.* **2018**, *514*, 164−175.
(25) McCoy, A. B.; Dzugan, L. C.; DiRisio, R. J.; Madison, L. R. Spectral Signatures of Proton Delocalization in $H^+(H_2O)_{n=1-4}$ Ions. *Faraday Discuss.* **2018**, *212*, 443−466.
(26) Yu, Q.; Bowman, J. M. Communication: VSCF/VCI Vibrational Spectroscopy of $H_7O_3^+$and $H_9O_4^+$ Using High-Level, Many-Body Potential Energy Surface and Dipole Moment Surfaces. *J. Chem. Phys.* **2017**, *146*, 121102.
(27) Dzugan, L. C. *Theoretical Treatments of the Effects of Low Frequency Vibrations on OH Stretches in Molecules and Ion-Water Complexes That Undergo Large Amplitude Motions*; Ph.D. thesis; The Ohio State University: 2017.
(28) Finney, J. M.; DiRisio, R. J.; McCoy, A. B. Guided Diffusion Monte Carlo: A Method for Studying Molecules and Ions That Display Large Amplitude Vibrational Motions. *J. Phys. Chem. A* **2020**, *124*, 9567−9577.
(29) Petit, A. S.; Ford, J. E.; McCoy, A. B. Simultaneous Evaluation of Multiple Rotationally Excited States of H_3^+, H_3O^+, and CH_5^+ Using Diffusion Monte Carlo. *J. Phys. Chem. A* **2014**, *118*, 7206−7220.
(30) Anderson, J. B. Quantum Chemistry by Random Walk. H ^2P, $H_3^+ D_{3h}{}^1A_1'$, $H_2{}^3\Sigma_u^+$, $H_4{}^1\Sigma_g^+$, Be ^1S. *J. Chem. Phys.* **1976**, *65*, 4121−4127.
(31) Suhm, M. A.; Watts, R. O. Quantum Monte Carlo Studies of Vibrational States in Molecules and Clusters. *Phys. Rep.* **1991**, *204*, 293−329.
(32) Lee, V. G. M.; Madison, L. R.; McCoy, A. B. Evaluation of Matrix Elements Using Diffusion Monte Carlo Wave Functions. *J. Phys. Chem. A* **2019**, *123*, 4370−4378.
(33) McCoy, A. B.; Diken, E. G.; Johnson, M. A. Generating Spectra from Ground-State Wave Functions: Unraveling Anharmonic Effects in the $OH^- \cdot H_2O$ Vibrational Predissociation Spectrum. *J. Phys. Chem. A* **2009**, *113*, 7346−7352.
(34) Guasco, T. L.; Johnson, M. A.; McCoy, A. B. Unraveling Anharmonic Effects in the Vibrational Predissociation Spectra of $H_5O_2^+$and Its Deuterated Analogues. *J. Phys. Chem. A* **2011**, *115*, 5847−5858.
(35) Lin, Z.; McCoy, A. B. Investigation of the Structure and Spectroscopy of H_5^+Using Diffusion Monte Carlo. *J. Phys. Chem. A* **2013**, *117*, 11725−11736.
(36) Wilson, E. B.; Decius, J. C.; Cross, P. C. *Molecular Vibrations*; Dover: New York, 1955.
(37) McCoy, A. B. Curious Properties of the Morse Oscillator. *Chem. Phys. Lett.* **2011**, *501*, 603−607.
(38) Huang, X.; Carter, S.; Bowman, J. M. *Ab initio* Potential Energy Surface and Rovibrational Energies of H_3O^+ and its Isotopomers. *J. Chem. Phys.* **2003**, *118*, 5431−5441.
(39) Huang, X. Private communication.
(40) Colbert, D. T.; Miller, W. H. A Novel Discrete Variable Representation for Quantum Mechanical Reactive Scattering via the S-matrix Kohn Method. *J. Chem. Phys.* **1992**, *96*, 1982−1991.
(41) McCoy, A. B.; Hinkle, C. E.; Petit, A. S. Studying Properties of Floppy Molecules Using Diffusion Monte Carlo. In *Advances in Quantum Monte Carlo*; Tanaka, S., Rothstein, S. M., Lester, W. A., Eds.; ACS Symposium Series 1094, 2012; Vol. *4*; pp 145−155.
(42) Louck, J. D.; Galbraith, H. W. Eckart Vectors, Eckart Frames, and Polyatomic Molecules. *Rev. Mod. Phys.* **1976**, *48*, 69−106.
(43) Eckart, C. Rotating Axes and Polyatomic Molecules. *Phys. Rev.* **1935**, *47*, 552−558.
(44) Frisch, M. J.; Trucks, G. W.; Schlegel, H. B.; Scuseria, G. E.; Robb, M. A.; Cheeseman, J. R.; Scalmani, G.; Barone, V.; Petersson, G. A.; Nakatsuji, H.; et al. *Gaussian 16, Revision A.03*; Gaussian Inc.: Wallingford. CT; 2016.

https://doi.org/10.1021/acs.jpca.1c05025
J. Phys. Chem. A 2021, 125, 7185−7197

(45) Liu, D.; Haese, N. N.; Oka, T. Infrared Spectrum of the ν_2 Vibration-Inversion Band of H_3O^+. *J. Chem. Phys.* **1985**, *82*, 5368−5372.
(46) Vaden, T. D.; Lisy, J. M.; Carnegie, P. D.; Dinesh Pillai, E.; Duncan, M. A. Infrared Spectroscopy of the $Li^+(H_2O)Ar$ Complex: the Role of Internal Energy and its Dependence on Ion Preparation. *Phys. Chem. Chem. Phys.* **2006**, *8*, 3078−3082.
(47) Boyer, M. A.; Marsalek, O.; Heindel, J. P.; Markland, T. E.; McCoy, A. B.; Xantheas, S. S. Beyond Badger's Rule: The Origins and Generality of the Structure−Spectra Relationship of Aqueous Hydrogen Bonds. *J. Phys. Chem. Lett.* **2019**, *10*, 918−924.
(48) DiRisio, R. J.; Lu, F.; McCoy, A. B. GPU-Accelerated Neural Network Potential Energy Surfaces for Diffusion Monte Carlo. *J. Phys. Chem. A* **2021**, *125*, 5849−5859.

https://doi.org/10.1021/acs.jpca.1c05025
J. Phys. Chem. A 2021, 125, 7185−7197